HHS Public Access

Author manuscript

Nat Neurosci. Author manuscript; available in PMC 2015 April 01.

Published in final edited form as:

Nat Neurosci. 2014 October ; 17(10): 1371–1379. doi:10.1038/nn.3797.

Gamma-range synchronization of fast-spiking interneurons can enhance detection of tactile stimuli

Joshua H. Siegle[*,1,2], **Dominique L. Pritchett**[*,1,2,3], and **Christopher I. Moore**[1]

[1]Dept. of Neuroscience and Institute for Brain Science, Brown University, Providence, RI

[2]Dept. of Brain and Cognitive Sciences, Massachusetts Institute of Technology, Cambridge, MA

Abstract

We tested the sensory impact of repeated synchronization of fast-spiking interneurons (FS), an activity pattern thought to underlie neocortical gamma oscillations. We optogenetically drove "FS-gamma" while mice detected naturalistic vibrissal stimuli and found enhanced detection of less salient stimuli and impaired detection of more salient ones. Prior studies have predicted that the benefit of FS-gamma is generated when sensory neocortical excitation arrives in a specific temporal window 20-25 ms after FS synchronization. To systematically test this prediction, we aligned periodic tactile and optogenetic stimulation. We found that the detection of less salient stimuli was improved only when peripheral drive led to the arrival of excitation 20-25 ms after synchronization and that other temporal alignments either had no effects or impaired detection. These results provide causal evidence that FS-gamma can enhance processing of less salient stimuli, those that benefit from the allocation of attention.

Neocortical oscillations in the gamma range (~30–80 Hz) are hypothesized to benefit sensory processing, a prediction that has generated significant debate. In support of this view, elevated gamma activity is correlated with the allocation of attention[1-4], and predicts enhanced performance on sensory detection tasks[5-7]. Further support comes from a variety of computational studies that have found that realistic modeling of gamma—emerging from synchronous activity in fast-spiking interneurons—can enhance the relay of signals in simulated neural networks[8-12].

These different lines of evidence suggest that gamma expression could explain some of the functional consequences of shifting attention. Specifically, the allocation of attention augments neural and perceptual responses to subthreshold or liminal inputs, the stimuli that require an additional boost for effective processing. However, as emphasized in a number of

Correspondence: Christopher Moore (christopher_moore@brown.edu).

*These authors contributed equally to this work.

[3]Present address: Champalimaud Centre for the Unknown, Lisbon, Portugal

Supplementary Information: See separate document for supplementary figures and methods.

Author Contributions: J.H.S., D.L.P., and C.I.M. designed the experiments. J.H.S. designed the implants and performed the viral injections. D.L.P. and J.H.S. designed the behavioral rig and oversaw training. J.H.S. and D.L.P. analyzed the data. J.H.S., D.L.P, and C.I.M. made the figures and wrote the manuscript.

studies, the relationship between gamma and enhanced processing associated with attention may be purely correlative, an epiphenomenal consequence of increased excitability in the neocortex[4,13,14]. This debate surrounding gamma has, to date, only been informed by correlative data. There has not yet been a direct causal examination of the impact—either positive or negative—of realistic gamma oscillations on perception.

A mechanistic understanding of the circuit-level activity patterns driving neocortical gamma is essential to considering its potential role in sensory processing, as well as to guiding causal interventions to test this dynamic. Correlative, causal, and computational evidence indicate that gamma in the 30–80 Hz range depends on synchronous activity of fast-spiking interneurons (FS)[10,15-21]. Coincident FS activity drives a period of concentrated inhibition, the relaxation from which creates a "window of opportunity" for adjacent pyramidal neurons to relay signals to downstream targets[22]. These excitatory spikes recruit nearby FS, thereby initiating the next gamma cycle[21]. The time constant of this inhibition (on the order of ∼15 ms) explains why gamma occurs in the 30–80 Hz range[23]. *In vivo* data supporting this mechanism have shown phase-locking of FS and pyramidal neurons during periods of high-amplitude gamma activity[17]. Further, selective optogenetic drive of FS *in vivo* entrains a rhythm that emulates many properties of endogenous gamma[19,20,24,25]. Because the mechanism generating gamma is inherent to understanding this phenomenon[10,21], throughout we refer to "FS-gamma." The present findings pertain to gamma emerging through FS synchronization, and not simply to electrophysiological activity in this frequency range. The LFP measurements that are typically used to characterize gamma are considered to be a consequence of this underlying mechanism.

In the present study, we examined the behavioral impact of directly entraining FS-gamma in primary sensory neocortex. To test this question in a well-controlled model, we selectively activated FS at 40 Hz in the barrel cortex of mice engaged in detecting vibrissal deflections. Barrel cortex is required for detection of such passive vibrissal stimuli[26-28], making this target appropriate for measuring the impact of realistic FS-gamma on perception. We found that endogenous gamma at stimulus onset predicted detection of naturalistic tactile stimuli, specifically for the detection of less salient input. When we used light pulses to entrain peri-stimulus FS, we similarly found improved detection of less salient naturalistic stimuli. To test whether this improvement was a product of more general transformations resulting from increased inhibitory tone, or whether it required access to the cyclical window of optimal processing generated by FS-gamma, we tested the detection of 40 Hz vibrissae deflections presented at temporal lags relative to the induced FS synchrony. In this artificial condition, gamma also selectively enhanced detection of less salient stimuli. Further, improved detection was only observed when the relative timing of feed-forward, sensory-driven excitation arrived in the window of opportunity created by prior FS synchronization. A limited sample of single unit recordings from layer II/III showed that induction of FS-gamma led to temporal sharpening that predicted behavioral benefit, but that firing rate averaged across this population did not increase, indicating that generic increases in rate are not a sufficient explanation for our findings. Neither rate nor temporal changes predicted a behavioral deficit that was observed at one temporal lag in the artificial stimulus condition, indicating that population-level transformations in layer II/III cannot be simplistically

interpreted as the sole driver of the perceptual transformations observed. In sum, these data provide correlative and causal evidence that local FS-gamma can enhance neocortical processing for harder-to-perceive stimuli, consistent with a role for this dynamic in behavioral states such as increased attention.

Mice can detect vibrissal deflections

We trained head-fixed mice to respond to 400 ms sequences of vibrissae deflections. These sequences were either stochastic ("naturalistic" stimulation) or 40 Hz pulses of uniform amplitude. If mice licked a reward spout within 500 ms of the first deflection, a drop of water was delivered (Fig. 1a). Mice sustained performance of the detection task consistently over weeks to months, with an average of 495 ± 96 trials per session (N = 8 mice; 27,534 ± 11,483 total trials per mouse). In interleaved trials, optogenetic drive was applied to FS, as described in greater detail below. Mice did not respond directly to this stimulation, showing nearly identical falsealarm rates on catch trials with lightpresent or absent (Fig. 1b; N = 8 mice; 0.22 ± 0.04 versus 0.21 ± 0.06; P = 0.84, Wilcoxon signed-rank test). Further, reaction times on "hit" trials were also indistinguishable during light-present and light-absent trials (211 ± 32 ms versus 210 ± 32 ms, respectively; P = 1.0, Wilcoxon signed-rank test).

Gamma is present in spontaneous SI activity

Gamma oscillations have previously been observed in rodent primary somatosensory neocortex (SI), both during baseline conditions[29,30] and in response to sensory drive[31,32]. These oscillations also arise in SI *in vitro* when stimulating pyramidal cells of the upper layers with ramping optogenetic stimuli[33,34]. Using chronically implanted stereotrodes in layer II/III, we recorded local field potential (LFP) activity while mice performed the detection task. The average pre-stimulus power spectra for 2 s intervals of inter-trial data averaged over an entire session showed a typical 1/f falloff, and did not contain peaks in the gamma range (Fig. 2a). This finding replicates recent reports in mouse barrel neocortex using this analysis method[35]. When looking at finer temporal scales, however, distinct bouts of spontaneously occurring increases in 30–80 Hz power were evident during the pre-stimulus period. Examples of these distinct epochs are illustrated in Fig. 2b and Supplementary Fig. 1. These bouts of gamma were identifiable in the raw LFP traces and in time-frequency spectrograms computed by either wavelet and Fourier transforms. They were detected at a rate of 0.89 Hz during inter-trial intervals without licking.

Multiunit and single-unit firing patterns were strongly modulated as a function of the phase of spontaneous gamma LFP power (Fig. 2c). Multiunit spike activity was concentrated at the trough of the LFP (mean phase across electrodes = 182.2 ± 26.9°, 180° indicates trough). This alignment and increase in phase-locking replicates many prior studies[1,4,6,17,30,36], indicating that the endogenous gamma that occurs in mouse barrel neocortex is associated with the same transformations observed in monkey higher visual neocortex[1] and ferret frontal neocortex[17]. This pattern of phase-locking of FS is also consistent with computational studies indicating the importance of synchrony in this cell class for the generation of naturally-occurring gamma[8,10,21,37], and with recent optogenetic data from mouse SI showing that selective drive of FS generates naturalistic gamma *in vivo*[19,20,25].

Optogenetically entrained gamma in awake mice

We brought gamma oscillations under experimental control by expressing the gene for channelrhodopsin-2, a light-gated cation channel (H134R variant), in parvalbumin-positive (PV) cells in the upper layers of the neocortex (Supplementary Fig. 2). In this layer, PV neurons are uniformly FS[19]. We emulated naturally occurring bouts of gamma by presenting 1 ms light pulses at 40 Hz for 600 ms. The light stimulus began 100 ms prior to the onset of vibrissal deflections, and ended 100 ms after (Fig. 1a). Light power at the surface of the cortex was 30 mW/mm^2, a lower level than that used in a previous study from our lab[19].

This optical input drove robust gamma entrainment in the LFP of awake mice (Fig. 3a) and short-latency action potentials in the multiunit activity (Fig. 3b). Optogenetic stimulation induced a 40 Hz peak in the LFP power spectral density (Fig. 3c), consistent with prior findings in anesthetized preparations[19,20,25]. Light pulses activated well-isolated FS, with evoked spikes concentrated between 2–3 ms after the onset of the laser (Fig. 3d), similar to previous findings[19,25]. We refer to these effects as “entrained” FS-gamma because the network impact of these oscillations on spiking mimics physiological gamma *in vivo*[17,19] (Fig. 2c) and optogenetic manipulation of this type can be used to phase-reset ongoing endogenous gamma oscillations[19]. The observed effects are consistent with FS activation, rather than a light-induced artifact at the electrode interface, as such artifacts are positive-going in input-inverted recordings (same direction as spikes), begin precisely at the time of light onset, and do not suppress spike activity[24].

Acquisition and characterization of vibrissal stimuli

To test the association of endogenous and entrained gamma with the detection of vibrissae deflections possessing natural stimulus statistics, we recorded the motions of an *ex vivo* vibrissa contacting a textured, rotating surface, and presented these patterns to behaving mice (Fig. 4a; Supplementary Fig. 3a). Using this approach, we generated 17 distinct “movies” of vibrissal motion to replay for psychophysical testing. High-velocity micro-motions are a common feature of vibrissal motion during surface contact, including during free behavior[38,39], and are widely regarded as a key driver of salience in the vibrissa sensory system. Neurons in SI are more effectively driven by higher velocity vibrissal motions[40], higher velocity of small amplitude motions predicts increased behavioral detection probability[41], and individual high velocity micro-motion events drive spiking in SI awake, freely behaving rodents[42]. The frequency of vibrissal motion for our stimuli was 180–200 Hz (Fig. 4b). The 17 natural stimuli movies were typified by the presence of high-frequency micro-motions, with a mean peak velocity of $1.75 \pm 0.41 \times 10^3$ degrees/s and maximal peak velocity of $5.53 \pm 1.73 \times 10^3$ degrees/s, (Fig. 4c). The occurrences of these micro-motions were evenly distributed relative to the timing of entrained FS-gamma, with no bias in alignment to a phase or temporal delay of optogenetic drive (Fig. 4d).

Four mice were presented with these 17 naturalistic velocity profiles interleaved with the periodic stimuli described below. To ensure that all trials were drawn from epochs in which mice were actively performing the task, we only analyzed blocks of trials in which behavioral performance was high (d' was above 1.25; Fig. 1a, Supplementary Fig. 4). We

also eliminated trials in which mice licked during a 1.5-second interval before trial onset. These filtering steps left 27.9 ± 9.0% of the original trials in our analysis, with a minimum of 469 trials per mouse in the naturalistic stimulation condition.

The 17 natural stimuli were not equivalent in terms of their detectability, with mean d' across animals ranging from 1.57 ± 0.47 to 2.66 ± 0.55. Consistent with prior psychophysical studies[41], stimulus detectability was correlated with higher velocity of vibrissal motion, as the integrated velocity envelope during the first 100 ms of stimulation significantly predicted d' (Fig. 4e–f, N = 17 stimuli; R^2 = 0.4468; P = 0.0034; mean reaction time across stimuli of 206 ± 20 ms).

Endogenous gamma predicts detection of less salient stimuli

Increased probability of sensory detection, and increased salience of sensory stimuli, have both been found to correlate with increased peri-stimulus gamma[6,43]. We similarly found that peri-stimulus gamma in SI predicted detection of vibrissal motion for less salient sensory stimuli. Our natural stimuli showed a non-significant broadband increase in LFP power during the peri-stimulus onset period (−200 to 50 ms, relative to vibrissal onset at 0) versus a baseline period (−450 to −200 ms) (Fig. 5a). When we compared the power spectra for hit and miss trials, gamma (30–50 Hz) was higher on hit trials in the peri-stimulus onset period for the least detectable sensory stimuli (Fig. 5b, bottom 50% of stimuli ranked according to detectability; N = 2 mice, 7488 trials; 2 mice rejected due to motion artifact in LFP; Bonferroni-corrected t-tests revealed significant difference in the 30–50 Hz band between hits and misses [$P = 4.3 \times 10^{-5}$ for mouse 1, $P = 6.8 \times 10^{-8}$ for mouse 2]).

Entrained FS-gamma and naturalistic stimulation

To directly test the impact of FS-gamma, we optogenetically drove FS in conjunction with naturalistic vibrissal stimulation. On trials where FS were driven, all mice showed a selective enhancement in detection of less salient stimuli (Fig. 5c). This observation is reflected in a negative correlation between the d' for the 17 natural stimuli (i.e., whether they were more salient for a given mouse) and the impact of entrained gamma on detection (Fig. 5b). We also applied the same manipulation in a PV-Cre negative control mouse, and saw no significant relationship between baseline performance and the impact of the optical drive (R^2 = 0.1842, P = 0.30; Supplementary Fig. 3b).

As a summary metric across mice of the impact of entrained FS-gamma as a function of stimulus detectability, we ranked the relative detectability of each of the 17 naturalistic stimuli for each animal, and then averaged the effect of this manipulation across these ordinal data (Fig. 5d). When considered as a function of relative detectability, 8 of 9 of the weakest stimuli showed increased detection with FS-gamma entrainment. We also found that 7 of 8 of the strongest stimuli were negatively impacted. This finding of impaired detection for salient stimuli is in apparent contrast to the lack of an association between endogenous gamma and hit or miss trials for highly salient natural stimuli, and a lack of an impact of driving FS-gamma on detection of highly salient periodic stimuli described below.

Entrained FS-gamma and periodic stimulation

The detection of less salient naturalistic stimuli was enhanced by entrainment of FS-gamma. This enhancement could have arisen from non-specific effects due to selective recruitment of FS, such as generalized arousal or enhanced signal-to-noise through the presence of increased inhibition. Alternatively, these effects could depend on enhancement of the specific temporal pattern of activity associated with FS-gamma. Specifically, prior computational studies[10,12] and experimental work[17,19,44] predict that excitatory input arriving ∼20–25 ms after an event of FS synchrony will be preferentially transmitted downstream, as a result of increases in synchrony across pyramidal neurons[12,18] and potentially by increases in their firing rate[10,12]. This optimal temporal window is predicted to be created by a variety of mechanisms, including but not limited to the relaxation of inhibition, as described further in the Discussion.

To test whether arrival of input during this window was associated with improved psychophysical performance, we combined 40 Hz FS activation with 40 Hz vibrissae deflections at a range of temporal alignments. Such precise alignment of an external stimulus with an internal gamma rhythm is unlikely to occur under natural conditions for several reasons, most importantly the fact that natural micro-motion patterns of vibrissae themselves created during surface contact will typically occur at much higher frequencies[38,39]. While artificial, this manipulation allowed us to directly test whether the timing of peripheral input relative to the optimal window created by FS-gamma shaped behavior.

We shifted the temporal lag between optical stimulus and sensory drive at 40 Hz by 5 ms steps, as in a prior study in anesthetized mice[19]. The latency from peripheral deflection to arrival of sensory-driven excitatory input to neocortex is ∼8–10 ms (Supplementary Fig. 5). As such, neocortical spikes evoked by vibrissal stimuli presented 12.5 msec after a light pulse would be predicted to arrive at the optimal window 20–25 ms after a prior bout of FS synchrony. For this temporal offset, the propagation delay between the periphery and neocortex positions the excitatory barrage from sensory drive to arrive after the decay of FS-driven inhibition, but just before the onset of the subsequent bout of inhibition (Fig. 6a).

In the first two mice trained, we presented stimuli of 9 different amplitudes to construct psychophysical response curves (Supplementary Fig. 4a). Based on these curves, we selected for intensive study a less salient amplitude of stimulation that generated intermediate detection rates. In these 2 subjects and in 6 subsequent mice, we randomly interleaved these threshold stimuli (∼800°/s peak velocity) with maximum-amplitude stimuli (∼2000°/s peak velocity). As in the naturalistic stimulation condition, we only analyzed trials from blocks in which d' was above 1.25 (minimum of 631 trials per mouse).

For less salient stimuli, detection was enhanced only for the 12.5 ms temporal offset condition (Fig. 6a). On these trials (represented in green), d' was higher than baseline for 7/8 mice and in the average (Fig. 6a mean difference from baseline = 0.23 ± 0.18, $P = 0.0391$; Wilcoxon signed-rank test with Bonferroni correction). Hit rate for the 12.5 ms offset was also enhanced and, as indicated above, no change in the false alarm rate on catch trials was

observed (Fig. 1b; Supplementary Fig. 6). To determine the likelihood that a single offset would show these effects under the hypothesis that entrained FS-gamma has no impact on performance, we applied a permutation test ($P < 0.01$, see Methods section). In contrast, for all temporal offsets other than 12.5 ms, d' did not differ from baseline or was significantly lower (7.5 ms offset, mean difference from baseline = –0.30 ± 0.21, $P = 0.0195$; Wilcoxon signed-rank test with Bonferroni correction). Thus, shifting entrained gamma oscillations by as little as 5 ms relative to sensory input led to significant variation in task performance. These data indicate that behavioral enhancement by optogenetic stimulation requires temporal processes specific to FS synchronization, rather than non-specific effects such as heightened arousal or general signal-to-noise transformations resulting from the manipulation.

We also quantified the impact of entrained FS-gamma on the detectability of maximum-amplitude, perceptually salient periodic stimuli, which had a baseline hit rate of 0.90 ± 0.03. In contrast to the enhancement observed with the less salient stimulus, we saw a non-significant trend towards enhancement at the 12.5 ms condition, and no significant changes for any other temporal offset with our optogenetic manipulation (Fig. 6b; $P = 0.711$, Friedman test). Further, when the performance of individual mice was analyzed, we found a range of detection levels for the less salient stimulus, resulting from the fact that stimulus intensity chosen based on performance of our first 2 mice was the same for all animals, and not scaled according to individual psychophysical abilities in each (Fig. 6c). The relative enhancement of detection by entrainment of FS-gamma at the 12.5 ms offset was predicted from the innate performance levels of each mouse. Those that performed inherently better in detecting the less salient stimulus, in the absence of the optogenetic manipulation, showed less benefit of entrained gamma ($N = 8$ mice; $R^2 = 0.64$, $P = 0.017$; Fig. 6d). The best-performing mouse, which had a baseline hit rate of 0.90 for less salient stimuli (identical to the mean detection rate for the “maximal” stimulus), had its performance negatively impacted by laser presentation. These inter-subject analyses further reinforce the finding that less salient stimuli were selectively benefitted by FS-gamma.

Physiological effects of vibrissa stimulation and FS-gamma

We analyzed 35 well-isolated regular-spiking cells, classified by waveform shape (Supplementary Fig. 7), or multi-unit activity (15 different electrodes, 3 mice). We only included units obtained from stereotrodes on which a rapid sensory-driven response was observed. Entrained FS-gamma transformed the spiking response in two ways that replicated prior findings in anesthetized mice[19]. First, for naturalistic and periodic stimulation, optogenetic manipulation suppressed baseline firing rates and decreased the average sensory-driven spike rate during the peri-stimulus period, independent of the relative alignment of sensory stimulation and light (Fig. 7a–e). Second, across all laser-to-vibrissae stimulus alignments, there was a significant increase in the vector strength (a measure of response periodicity of single units) during the peri-stimulus period (Fig. 7a–c,e), indicative of enhanced phase-locking to entrained FS-gamma. Third, in agreement with prior findings[19], delivering the sensory stimulus 12.5 ms after each laser pulse resulted in a selective enhancement in spike precision (a measure of the width of the multiunit evoked response to the first vibrissae deflection) and the strongest enhancement of gamma power in

spike time distributions (Fig. 7e, Supplementary Figure 8). This finding is consistent with the arrival of sensory-driven excitatory input ~8–10 ms post-stimulation, which aligns the excitatory spikes to the optimal phase of post-inhibitory decay (Fig. 6a; Supplementary Fig. 5).

The absence of mean increases in firing rate across our sample—we observed, in fact, significant *decreases* in mean rate—directly indicate that population-level gain cannot explain our behavioral findings. We note that a small subset of RS did show rate increases, indicating that firing enhancement in a select group could have provided sensory benefit. In contrast, enhanced temporal sharpening did predict conditions that led to behavioral benefit for the natural and artificial stimuli. Neither rate nor temporal transformations predicted the decreased detectability observed with the 7.5 ms latency artificial alignment condition (Fig. 6a), underscoring that population-level transformations of the layer II/III neurons we sampled cannot provide a sufficient explanation for the full range of perceptual results.

Discussion

The current experiments tested the behavioral impact of mechanistically realistic FS-gamma in a local neocortical circuit. Endogenous expression of higher gamma power predicted the detection of less salient sensory stimuli, and driving FS at 40 Hz enhanced the detection of less salient sensory stimuli. This finding was replicated across naturalistic and periodic stimuli. Stimuli that were highly salient were not benefitted by FS-gamma. Detection of highly salient periodic stimuli was neither aided nor penalized by entrained FS-gamma, and endogenous gamma did not predict enhanced or decreased detection of highly salient naturalistic stimuli, though FS-gamma did impair detection of these naturalistic inputs. Studies in rodents[26-28] have shown that transient silencing or lesioning of SI impairs the detection of less salient tactile stimuli. The present findings are consistent with the view that FS-gamma beneficially impacts processing of hard-to-perceive stimuli that require neocortical circuitry, and especially those that may require the allocation of attention to be detected consistently.

FS-gamma generates windows of opportunity for spiking

A simple conceptual framework can explain how emulated FS-gamma enhanced detection of the naturalistic and periodic stimuli used here (Supplementary Fig. 9). Prior studies have predicted that synchronous activation of FS should create a “window of opportunity” 20-25 ms later, and that inputs arriving from the periphery during this window should show increased gain and/or synchrony. Below, the motivations for these mechanistic predictions are discussed, but considering the basic conceptual framework requires only the a-mechanistic prediction that such a window exists.

High-velocity micro-motions are widely regarded as a key driver of sensory responses and behavioral detection in the vibrissa sensory system[41,42]. During the periodic stimulation condition in the present experiments, high-velocity micro-motions repeatedly occurred at specific latencies relative to FS synchrony. Given the well-documented lag of ~8–10 ms for transmission of high-velocity vibrissal motions from periphery to SI (Supplementary Fig. 5),

the 12.5 ms latency (green) drove peripheral inputs arriving in neocortex 20–25 ms after FS synchronization, during the predicted optimal window. Under the “artificial” conditions of alignment in the periodic stimulation task, only sensory stimulation arriving at this latency should access this window. Therefore, it is the only latency that would be predicted to drive enhanced relay and, in turn, improved behavioral performance.

In contrast, naturalistic stimuli have a much higher rate of high-velocity micro-motions. In the present experiment, mean vibrissal frequencies fell in the range of 180–200 Hz, corresponding to ∼10 such events per 25 ms FS-gamma cycle. As diagrammed in Figure 4d and Supplementary Figure 9, these high-velocity micro-motions occurred at random times relative to the beneficial window created by FS synchronization. However, because micro-motions occur at a high rate, they can consistently drive peripheral input that arrives during the beneficial window and yield enhanced sensory processing in the presence of FS-gamma. The enhanced detection observed when combing FS-gamma with the least salient naturalistic stimuli indicates that there is not an apparent a penalty for also having inputs arrive outside the beneficial window. This finding is in contrast to the more artificial periodic stimulation condition with a 7.5 ms latency, in which all inputs arrived just before the window and resulted in impaired performance. Put another way, the conceptual framework predicts that naturalistic stimuli received the benefit of FS-gamma presence by having high-velocity micro-motions that drove activity in the optimal window, but there was no perceptual penalty for extra high-velocity micro-motions at other latencies.

An open question is why detection of more salient naturalistic stimuli was suppressed by entrained FS-gamma. In apparent contrast, highly salient periodic stimuli were not impaired, and endogenous expression of higher gamma power did not predict impaired detection of highly salient naturalistic stimuli. Baseline detection rates for highly salient periodic and naturalistic stimuli were around 90% (Fig. 5d Supplementary Fig. 6), so ceiling effects alone cannot explain this discrepancy. Further experiments will be required to directly address this issue.

Our findings and this conceptual framework indicate that FS-gamma will benefit perception if sensory inputs are less salient, and consist of a high rate of peripheral events (as in many vibrissal or auditory natural scenes), or a consistent, tonic presence of input generating high-frequency drive (such as during sustained visual input while fixating for hundreds of milliseconds between saccades). Stochastic more sparse afferent input could also access this window. The present results suggest that only stimuli occurring at the same frequency as FS-gamma, and with the “wrong” latency offset, would be penalized by the emergence of this dynamic. In concept, however, such stimuli should be relatively rare in natural sensation.

Potential mechanisms underlying the perceptual benefits

Generation of FS-gamma has been hypothesized to benefit processing by producing enhanced firing rate in response to sensory stimuli (increased gain), and/or synchronization of local pyramidal activity. Several mechanisms have been proposed for how FS-gamma could lead to firing rate gain, including cellular-level induction of enhanced excitability resulting from a prior deep inhibition[10,44,45]. Circuit-level mechanisms have also been

proposed, including increased pyramidal excitability through decreased feed-forward recruitment of FS in the period immediately following synchronous FS activation[12]. Synchronization of pyramidal activity—with or without concomitant rate changes—has also been a proposed consequence of FS-gamma expression, and could occur through the enhanced temporal precision enforced by multiple cycles of inhibition. Firing probability will be reduced during the peak of deep inhibition generated by synchronous FS activation, and again by the following cycle of inhibition, leaving the "window of opportunity" for pyramidal activation[17]. Limiting the temporal occurrence of pyramidal firing to this window should increase synchrony, and synchronous activation could benefit downstream relay by an increase in the probability of driving spikes in downstream targets. Supplementary Fig. 10 provides a graphical representation of the impact of these predictions and further description of them.

Entrained FS-gamma did not increase net firing rate

In the limited sample of single units from layer II/III recorded in the present study, we did not observe widespread increases in rate in the presence of entrained FS-gamma, and instead observed significant decreases in mean rate (Figure 7c,e). This finding is inconsistent with the view that rate increases across the local population (e.g., layer II/III of the relevant neocortical column) are required to drive the perceptual enhancement we observed. Our limited sample did reveal gain increases in a few RS, posing the possibility that FS-gamma driven rate enhancement in a sparse, maximally informative subset of neurons could be crucial to behavior, even though the net effect was suppression.

In contrast to the absence of population rate effects, we observed enhanced temporal precision in sensory evoked responses that predicted enhanced performance in the naturalistic and periodic stimulus conditions. These findings imply that local synchrony could underlie the perceptual benefit observed. However, neither rate changes nor temporal precision changes predicted the decreased detection probability observed at the 7.5 ms latency. This failure of local neural transformations to predict positive and negative impacts on behavior underscores the limitations of the current data set, and more generally the likelihood that the effect of local FS-gamma on behavior is a network-level phenomenon, and not simply the altered readout of a single local neural-population–level metric.

Interpretations relative to other recent reports

Recent studies examining the neural correlates of sensory performance in rodents have come to a variety of conclusions regarding the relative importance of rate transformations for behavioral success. In a recent study, O'Connor and colleagues concluded that the rate of layer IV firing of barrel neocortex neurons predicted detection of vibrissal contact with a pole, independent of the phase of vibrissal position at the time of the rate increase[46]. Similarly, Sachidhanandam and colleagues found that detection of highly salient vibrissal deflections was predicted by increased firing in layer II/III neurons that was not temporally locked to the stimulus, occurring in a window 50–400 ms after initial passive vibrissa motion. High-frequency (200 Hz) optogenetic activation of FS during this epoch suppressed behavioral performance[28]. Detection of direct optogenetic stimulation by mice has also

suggested that rate, and not temporal pattern or synchronization, are exclusively predictive of performance. Histed and colleagues[47] recently reported that the rate of activation resulting from optogenetic drive of excitatory neurons across neocortical layers in V1 was the sole predictor of detection of these stimuli. They failed to observe a benefit of patterning excitatory drive in the beta and gamma frequency ranges.

In potential contrast to these recent results, our findings do not suggest that mean rate increases across a local population predict perceptual success. However, the present findings are supported by a recent study from Doron and colleagues[48]. This study found that behavioral detection of single neuron stimulation was not simplistically predicted by rate increases, with evoked firing rates of 30 Hz better detected than rates of 90 Hz. Further, they observed that direct stimulation of FS was more effective in driving detection than direct stimulation of pyramidal neurons. This result agrees with our finding that FS drive at 40 Hz can systematically enhance detection probability. In further agreement with the present results, detection of the change in the orientation of visual input in mice was also enhanced by optogenetic FS drive of area V1, although this study did not measure whether gamma LFP increases were induced by their optogenetic stimuli[49].

Reconciliation of these apparently disparate results could arise from experimental differences. The current study probed layer II/III in a passive detection task, in contrast to manipulation of layer IV dynamics in a sensorimotor task by O'Connor et al.[46] and the stimulation of excitatory neurons across layers in Histed and Maunsell[47]. If population-level rate increases in deeper layers predict enhanced detection, while they do not for layer II/III, the present findings may be consistent. While similar in paradigm, Sachidhanandam et al.[28] probed only supramaximal stimuli in their experiment, and did not attempt to emulate FS-gamma, instead applying FS stimulation at 200 Hz, differences that could readily account for their dissimilar findings to our own.

Although these potential explanations could account for the different conclusions reached across studies, the similarity in the findings of Doron et al.[48] and the present results suggest that, at least under the experimental conditions in these studies, mean increases in rate across larger populations of neurons are not a requisite predictor of detection success, and that the dynamics driven by FS recruitment are an effective mechanism for enhancing relay.

A role for FS-gamma can be distinct from a role in binding

Correlative studies have shown that local neocortical gamma oscillations are often present at an appropriate time to enhance perceptual processing. The allocation of attention to a specific position in space leads to increased gamma expression during stimulus presentation in the associated region of area V4[1,6]. These findings, and theoretical and empirical studies implicating fine-timescale synchronization across dispersed representations, coincide with a hypothesis that gamma-mediated temporal organization underlies the binding of images into a coherent percept[50]. This hypothesis, as well as related predictions linking gammatimescale activity to the encoding of stimulus features, has been criticized as inconsistent with the fluctuations in the precise frequency of gamma observed in area V1 with changes in stimulus salience[14].

These recent results showing gamma fluctuations do not contradict a different view about the potential benefit of gamma, supported by the present findings, that increased FS-gamma in a local neocortical circuit could enhance the relay of stimuli to benefit detection[10,12,44]. Under this view, transformations in pyramidal synchrony or increases in local firing rate associated with FS-gamma can increase the probability of downstream relay. In agreement with this prediction, higher levels of gamma over human occipital lobe predict enhanced detection of change[7], and similar increases in human somatosensory neocortex predict heightened detection of innocuous input[5] and the salience of painful stimuli[43]. Further, local gamma expression in V1 predicts increased firing in synaptic recipients in V2 with aligned receptive fields[36]. The present study supports this predicted role for FS-gamma, while the psychophysical demands of the present experiments do not directly test a role in binding or encoding by this dynamic.

Implications for further study

The current study was designed to test the behavioral impact of emulating a natural dynamic, the repeated cyclical synchronization of FS in the gamma frequency range. While the present experiments are conclusive in showing enhancement of sensory detection by entrained FS-gamma, and the specific requirement for accessing a window of opportunity to achieve this enhancement, they are not conclusive as to the specific neural mechanisms mediating this benefit. Systematic examination of this question will require the local measurement of synchronization and gain of well-isolated single units localized to additional specific cell layers in SI. Simultaneous interrogation of downstream activity in cortical and subcortical targets—including correlative recording and causal control—will be necessary to determine what impact these transformations have on relay.

Another key question and topic for further study is whether the periodicity and frequency range of FS-gamma matters for behavioral benefit, or whether individual events of FS synchronization, potentially occurring stochastically and with greater or lower frequency, can drive the same effects. Our conceptual model does not require a subsequent cycle of synchronized FS activity after the optimal temporal window for relay of signals to benefit (Supplementary Figure 9). Further, as discussed above, recent work by Histed and colleagues[47] suggests that rates of activity in the gamma range are not preferentially relayed, though work by Doron and colleages[48] suggests that such patterning may be beneficial. Our own computational modeling[12] has predicted that the timing of the next event of FS synchrony—e.g., 25 ms after the prior event—may be optimal in enhancing the efficiency of neocortical relay, by preventing the expression of spikes that would not have contributed to relay occurring outside the optimal temporal window. From this perspective, the rate of FS-gamma at 30–80 Hz may be optimal because it is the fastest rate at which cycles of a beneficial individual temporal transformation can be realized, not because the frequency per se carries information about the stimulus.

Conclusion

The current results directly address a long-standing debate in neocortical function, whether FS-gamma can impact sensory processing (either positively or negatively). While theoretical

studies have long suggested a role for this dynamic in processes such as attention, the evidence in support of this view has so far been correlative. Arguments against a possible role for FS-gamma have included mechanistic propositions, such as the view that the biophysical properties of neocortical neurons are not suited to benefit from this dynamic[13], and information-processing perspectives, such as the view that neocortical transformations on such short timescales would not benefit read-out of perceptual signals[13,14]. Here, we provide causal evidence that FS-gamma can improve psychophysical performance, and that such enhancement requires transformations with temporal precision on the ∼5 ms timescale. The degree to which these findings generalize to other tasks and brain regions requires further study, as does detailed examination of the local and downstream transformations in neural activity driven by FS-gamma. Nevertheless, these results provide a unique existence proof that this dynamic can improve the relay of sensory signals through the neocortex.

Online Methods

Animals

All mice were male parvalbumin-Cre (PV-Cre) heterozygotes, derived from PV-Cre BAC transgenics back-crossed into a C57BL/6J line (gift from S. Arber, now available as Jackson Laboratory strain B6;129P2-*Pvalb*$^{tm1(cre)Arbr}$). Mice were 8–14 weeks old at the time of initial surgery (mean age = 11.5 ± 2.6 weeks). Animals were individually housed and maintained on a 12-hour reversed light/dark cycle (lights out at 9:00 AM or 12:00 PM). All experimental procedures and animal care protocols were approved by the Massachusetts Institute of Technology and Brown University Institutional Animal Care and Use Committees and were in accordance with NIH guidelines.

AAV vectors

ChR2[51] fused to the fluorescent protein mCherry was cloned in the antisense direction into pAAV-MCS (Stratagene) to create AAV DIO *ChR2-mCherry* (Supplementary Fig. 2). *ChR2-mCherry* was flanked by a pair of canonical loxP sites (Tsien et al., 1996) and a pair of mutated lox2272 sites. A woodchuck hepatitis B virus post-transcriptional element was placed in sense direction 5′ of the poly (A). Adeno-associated viral particles of serotype 2 were produced by the Vector Core Facility at UNC Chapel Hill.

Fiber-optic–electrode implants

Implants were constructed around a custom plastic base, designed in SolidWorks (Dassault Systems, Waltham, MA) and printed via stereolithography in Accura 55 plastic (American Precision Prototyping, Tulsa, OK). The plastic base held 8 electrodes around a central fiber optic cable (Doric Lenses, Quebec, Canada). Electrodes were made from 12.5 μm polyimide-coated nichrome wire (Kanthal, Halstahammar, Sweden), twisted and heated to form tetrodes or stereotrodes[52]. In three animals, the electrodes were stationary. In five animals, electrodes were fixed to laser-cut plastic springs (Pololu, Las Vegas, NV) individually driven by miniature screws[53]. Electrodes were attached to a custom electrode interface board (Sunstone, Mulino, OR) with gold pins (Neuralynx, Bozeman, MT). Individual electrodes were gold plated to an impedance of 200–400 kΩ. The fiber optic cable

had an inner diameter of 200 μm and a cladding diameter of 260 μm, and was terminated with a 1.25 mm metal ferrule (Supplementary Fig. 7).

Surgical procedure

Naïve mice were anesthetized with isofluorane gas anesthesia (0.75–1.25% in 1 L/min oxygen) and secured in a stereotaxic apparatus. The scalp was shaved, wiped with hair removal cream, and cleaned with iodine solution and alcohol. Following IP injection of Buprenex (0.1 mg /kg, as an analgesic) and dexamethasone (4 mg/kg, to prevent tissue swelling) and local injection of lidocaine, the skull was exposed with an incision along the midline. After the skull was cleaned, two small stainless steel watch screws were implanted in the skull plates anterior to bregma, one of which served as ground. Next, a ∼1.5 mm–diameter craniotomy was drilled over barrel cortex of the left hemisphere (1.5 mm posterior to bregma and 3.5 mm lateral to the midline). We did not target a specific barrel, but post-hoc analysis revealed that our implants were located near the rear of the barrel map, centered around the C2 column. Virus was delivered through a glass micropipette attached to a Quintessential Stereotaxic Injector (Stoelting). The glass micropipette was lowered through the dura to a depth of 450 μm below the cortical surface. A bolus of 1 μl of virus (AAV DIO ChR2-mCherry; 2×10^{12} viral molecules per ml) was injected into the cortex at 0.05 μl/min. After the injection, the pipette was held in place for 10 min at the injection depth and 10 min at a depth of 200 μm before being fully retracted from the brain. The fiber-optic–electrode implant (Supplementary Fig. 7a) was aligned with the craniotomy at an angle of 15° from vertical and lowered to the surface of the cortex, centered approximately 200 μm anterior to the injection site. If notable bleeding occurred during implantation, the surgery was aborted. Once the implant was stable, a small ring of dental acrylic was placed around its base. A drop of surgical lubricant (Surgilube) prevented dental acrylic from contacting the cortical surface. A custom head post made from durable plastic (APProto) was then affixed to the skull with adhesive luting cement (C&B Metabond). Once the cement was dry, the scalp incision was closed with VetBond (3M), and mice were removed from isoflurane. Mice were given 3–10 days to recover prior to the start of water restriction.

Stimulus delivery and behavioral control

Vibrissae were stimulated by computer-controlled movements of piezoelectric wafers (Noliac, Kvistgård, Denmark). Stimulations consisted of high-speed deflections in the dorsal direction with a raised cosine velocity profile (6 ms rising phase) or naturalistic velocity profiles based on actual vibrissa movements as described above and in the text. Vibrissae were held with a silk suture loop fed through a 4 mm, 21-gauge stainless steel cannula, which was attached to the piezoelectric wafer via a glass capillary tube (0.8 mm outer diameter). Several vibrissae were secured, centered around the C2 vibrissa, and gripped approximately 5 mm from the mystacial pad. Mice were photographed from above at the start of each session to confirm which vibrissae were stimulated. For maximum-amplitude deflections, vibrissae moved approximately 1 mm at the point of contact. All stimulation amplitudes were calibrated using a linear CCD array.

Water delivery was based on gravitational flow controlled by a solenoid valve (Lee Co., Westbrook, CT) connected with Tygon tubing. Mice received distilled water through a

plastic tube mounted on a piezoelectric wafer. This “lick tube” was positioned near the animal's mouth using a micromanipulator. The water volume was controlled by the duration of valve opening (30–60 ms), calibrated to give ∼8 μL per opening. Individual licks were detected by amplifying and thresholding the output of the piezoelectric wafer using a custom circuit board or Arduino microcontroller.

The light stimulus was delivered through a jacketed fiber-optic cable 200 μm in diameter and 2.5 m long with a numerical aperture of 0.22 (Doric Lenses, Quebec, Canada) connected to a 473 nm laser (Opto Engine, Salt Lake City, UT). Laser light passed through an adjustable neutral-density filter and a collimator (Thorlabs PAF-X-15-PC-A) before entering the fiber. The 2.5 m fiber was connected to the animal's head via two mating metal ferrules sheathed in a zirconia sleeve. Light loss for this connection was measured for each implant prior to surgery, and was around 50%. The amplitude of the light stimulus was calibrated daily with an optical power meter (Thorlabs PM100D with S120C sensor). Light power at the surface of the cortex was estimated to be ∼1 mW, or 30 mW/mm^2 for a 200 μm fiber, a lower level than that used in a previous study from our lab[19]. We wanted our optogenetic manipulation to modulate FS synchrony, rather than flood the cortex with inhibition. Because the fiber was not implanted into the brain, this irradiance was roughly the same throughout the craniotomy (1.5 mm diameter). To calculate the depth of light penetration, we used a model based on direct measurements in mammalian brain tissue[53] (http://www.stanford.edu/group/dlab/cgi-bin/graph/chart.php). Light power was strongest in layer II/III, falling off to 1.75 mW/mm^2 at a depth of 500 microns (∼layer IV).

All behavioral events, piezoelectric control, reward delivery, laser stimulation, and lick measurements were monitored and controlled by custom software written in LabVIEW or Matlab and interfaced with a PCI DIO board (National Instruments, Austin, TX).

Trial structure

On each trial with 40 Hz stimuli, vibrissae were stimulated for 400 ms at a single amplitude, varying between 0 (“blank” trials) and 1 mm (“maximal” trials). Amplitude did not vary within a given trial. For naturalistic stimuli, vibrissae were stimulated with one of seventeen 400 ms velocity profiles (main text and Supplementary Fig. 3). On laser-stimulation trials, 1 ms light pulses were delivered at 40 Hz for 600 ms. Vibrissae deflections began after the fourth light pulse. The precise timing of the vibrissae deflections relative to the light pulses varied across five temporal offsets in the periodic stimulus trials, but remained consistent within individual trials. For all sessions, inter-trial intervals were uniformly distributed between 4 and 6 s.

If mice licked the reward spout at any point up to 500 ms after the onset of the vibrissae stimulus, a drop of water was delivered. After a slight delay, any remaining water was removed via vacuum suction. This prevented mice from receiving reward that was not immediately preceded by a vibrissae stimulus. There was no punishment or time-out period for false alarms.

When the vibrissae were removed from the lasso, but the stimulator remained near the face, performance immediately dropped to chance levels. This indicates that mice were not

licking to some other aspect of the stimulus, such as auditory cues or vibrations transmitted through the table.

Behavioral training

Training began after at least 3 days of post-operative recovery and at least 7 days of water restriction (1 ml /d). All training sessions took place near the beginning of the animals' dark cycle. At the beginning of each session, mice were secured to the head post apparatus with their bodies placed inside a Falcon tube. For the first five training sessions, mice were head fixed for periods of 5 to 15 minutes and given water ad libitum, to allow them to accommodate to the experimental apparatus. Vibrissae stimulation was added during the next week of training. At first, post-stimulus reward was delivered regardless of the animal's response, to establish a contingency between vibrissae deflections and drops of water. During this week, training time was gradually increased to 45 minutes. As mice became accustomed to performing the task (at approximately day 10 of training), water was only delivered if the reward spout was licked within 500 ms of stimulus onset. Initially, all trials included maximum-amplitude stimuli, with no blank trials. On successive days, blank stimuli (up to 10%) were randomly interleaved and the probability of non-maximal stimuli was increased.

After reaching criterion on the training task, laser light stimulation was added on a subset of trials. Laser stimulation was given ∼100 ms preceding tactile stimulation for a duration of 600 ms (100 ms post stimulation) at ∼1 mW power on the cortical surface. 50% of trials included delivery of stimuli at a single “threshold” amplitude ranging from 20–40% of the maximum stimulus amplitude, with the same duration to peak amplitude (6 ms). 30% of trials were blank, with the remaining 20% of trials at maximum amplitude to keep the animals engaged in the task. On half of all trials, laser stimulation was presented at one of 5 temporal offsets (Fig. 6a). All trial types were randomly interleaved.

Mice that did not consume 1 ml of water during the training sessions were supplemented with water in their home cage several hours after the experiment finished.

Electrophysiology

Spikes and local field potentials were recorded using twisted-wire nichrome stereotrodes or tetrodes integrated into a custom implant[53,55] (Supplementary Fig. 7a). Recording electrodes were either implanted 300–400 μm from the surface of the cortex during surgery, or lowered to the same depth over the course of several days. Once they reached their final depth, electrodes were not moved for the remainder of the experiment. Throughout each recording session, broadband signals referenced to ground were digitized at 40 kHz (Recorder/64, Plexon, Dallas, TX). Electrophysiology data was synchronized with behavioral data via TTL pulses at the start of each trial.

We measured the delay between the onset of the first deflection and the appearance of the evoked response on our recording electrodes. We found the delay to be 8–10 ms, similar to previous reports[56-59] (Supplementary Fig. 5).

Histology

At the end of training, electrodes sites were lesioned with 15 μA of current for 10 s. Mice were transcardially perfused with 100 mM PBS followed by 4% formaldehyde in PBS. Brains were post-fixed for at least 18 h at 4 °C. 60 μm sections were mounted on glass slides with Vectashield (Vector Laboratories), coverslipped, and imaged with an upright fluorescent microscope (Supplementary Fig. 2b). Viral expression was confirmed in all animals ($N = 8$). Expression was generally limited to the upper layers of barrel cortex (II–IV). In one animal, expression was also observed in the lower layers (V and VI). Ventral/medial and anterior/posterior spread of the virus ranged between 0.3 and 1.0 mm, encompassing 1–3 barrel columns.

Behavioral analysis

Data analysis was performed in Matlab (Mathworks, Natick, MA). Raw data from LabVIEW or Matlab was converted to event times for behavioral analysis. Trials were first selected based on d' according to the following procedure: (1) hit rate and false alarm rates were calculated for blocks of 50 trials, slid in 1-trial intervals. A negative offset was added to the hit rate and an equal-but-opposite offset was added to false alarms, to prevent d' saturation. An offset of 0.04 was used for all analyses. Hit rate was capped at a minimum value equivalent to the offset and false alarm rate was capped at a maximum value equivalent to 1 minus the offset. (2) d' was calculated as Z (hit rate) – Z (false alarm rate), where Z stands for the inverse of the Gaussian distribution function (Supplementary Fig. 5). (3) For any blocks with d' above a value of 1.25, the middle trial was included in the analysis. If fewer than 25% of trials remained after this procedure was carried out, the subject was excluded from analysis (1/9 mice for periodic stimuli, 1/5 mice for naturalistic stimuli). This criteria was established prior to the start of experimentation.

After d' trial rejection, trials with pre-stimulus licks within 1.5 s of trial onset were also eliminated. Trials were selected from the remaining subset based on the parameters of the vibrissae and laser stimuli. Hit rate and d' were calculated for each animal for each set of parameters.

Because all mice were of the same genotype, and all experienced the same experimental conditions (except the four mice that did not receive the naturalistic stimulation), data collection and analysis were not performed blind to the conditions of the experiments.

Statistical analysis

P-values were obtained using nonparametric statistical tests, unless otherwise stated. Where there were more than two treatments per animal (such as the 5 stimulus-to-laser temporal offsets plus baseline conditions), the Friedman test was used (nonparametric version of a repeated-measures ANOVA). For post-hoc comparisons and any tests where we collapsed across temporal offsets, we used the one-sided Wilcoxon signed-rank test if the hypothesis was predicted by previous work (e.g., improved performance by the 12.5 ms offset), and a two-sided test otherwise. Whenever multiple tests were performed on the same dataset, we adjusted our P-values using the Bonferroni correction procedure. No statistical methods

were used to pre-determine sample sizes but our sample sizes are similar to those reported in previous publications[41,49].

To analyze the significance of the results from Figure 6, we also employed a permutation procedure to determine the likelihood that at least 7/8 animals would improve relative to baseline at any one temporal offset *and* at least 5/8 animals would have their best performance at that temporal offset, under the null hypothesis that our manipulation had no effect. For each round of the simulation, 5 temporal offsets + 1 baseline condition were randomly ordered for each of 8 mice. After 10,000 repetitions, we counted the total number of rounds in which the requirements were satisfied, and found the probability was always less than 0.01.

In one case (Fig. 5b), we used a *t*-test with Bonferroni correction to test significance. We used the Kolmogorov–Smirnov test to test for normality before applying this test ($P < 0.0005$).

Offline electrophysiological analysis

Continuous electrophysiological data from the Plexon system was either low-pass filtered (3rd-order Butterworth) and downsampled to 2 kHz or filtered between 600 and 6000 Hz (acausal FIR filter) and thresholded to extract spikes. Spikes were sorted offline using custom software written in Matlab (Simple Clust v0.5, available online at https://github.com/moorelab/simpleclust). Well-isolated single units were readily matched across days by eye; afterward, cell identity was confirmed using a waveform similarity metric[60]. In total, we isolated 43 units from 3 mice, which persisted an average of 3.29 ± 3.2 d each (range: 1 to 13 d). The distribution of units was as follows: 26 units from Mouse 1, 1 from Mouse 2, and 16 from Mouse 3. Cluster quality was quantified using L-ratio and isolation distance of the four peak heights of bandpass-filtered waveforms for each tetrode[61]. If putative single units had an L-ratio greater than 1 or an isolation distance less than 5, they were rejected. On average, our units had an L-ratio of 0.19 ± 0.20 and an isolation distance of 19.68 ± 15.42, similar to previously reported values for peak heights[62]. We used the peak-to-trough ratio and peak-to-trough separation on 600 to 6000 Hz filtered waveforms to classify cells as fast spiking or regular spiking. We found two distinct clusters of units, one with 35 regular-spiking cells and one with 8 fast-spiking cells (Supplementary Fig. 7d). A subset of well-isolated FS units (2 of 8) were activated by light.

Peri-stimulus firing rate was calculated as the mean firing rate between 30 ms and 400 ms after stimulus onset. Vector strength was calculated for the same period using the procedure described in[63]. Spike precision was calculated as the inter-quartile range of spike times within the first 25 ms of stimulus onset[64]. Spike precision was calculated only on multi-unit activity, as single-unit spike rates were not high enough to observe consistent peri-stimulus time histograms after the first vibrissae deflection. This is the same way that spike precision was measured in a previous paper from our lab[19].

Supplementary Material

Refer to Web version on PubMed Central for supplementary material.

Acknowledgments

We thank R. Clary, J. Feather, H. Farrow, R. Lichtin, S. Bechek, J. Klee, N. Padilla, and C. Burley for help running experiments. We are grateful to J. Cardin, U. Knoblich, M. Halassa, J. Ritt, J. Voigts, C. Deister, B. Higashikuibo, D. Meletis, and M. Carlén for technical assistance. We thank members of the Moore lab, M. Wilson, M. Andermann, R. Haslinger, N. Kopell, C. Börgers, R. Sekuler, and D. Sheinberg for their comments on the manuscript. This study was supported by a grant from the NIH to C.I.M., an NRSA Fellowship to D.L.P., and NDSEG and NRSA Fellowships to J.H.S.

References

1. Fries P, Reynolds JH, Rorie AE, Desimone R. Modulation of oscillatory neuronal synchronization by selective visual attention. Science. 2001; 291:1560–1563. [PubMed: 11222864]
2. Fries P, Womelsdorf T, Oostenveld R, Desimone R. The effects of visual stimulation and selective visual attention on rhythmic neuronal synchronization in macaque area V4. J Neurosci. 2008; 28:4823–4835. [PubMed: 18448659]
3. Bosman CA, et al. Attentional stimulus selection through selective synchronization between monkey visual areas. Neuron. 2012; 75:875–888. [PubMed: 22958827]
4. Ray S, Ni AM, Maunsell JH. Strength of gamma rhythm depends on normalization. PLoS Biol. 2013; 11:e1001477. [PubMed: 23393427]
5. Meador KJ, Ray PG, Echauz JR, Loring DW, Vachtsevanos GJ. Gamma coherence and conscious perception. Neurology. 2002; 59:847–854. [PubMed: 12297565]
6. Womelsdorf T, Fries P, Mitra PP, Desimone R. Gamma-band synchronization in visual cortex predicts speed of change detection. Nature. 2006; 439:733–736. [PubMed: 16372022]
7. Hoogenboom N, Schoffelen JM, Oostenveld R, Fries P. Visually induced gamma-band activity predicts speed of change detection in humans. Neuroimage. 2010; 51:1162–1167. [PubMed: 20307670]
8. Wang XJ, Buzsáki G. Gamma oscillation by synaptic inhibition in a hippocampal interneuronal network model. J Neurosci. 1996; 16:6402–6413. [PubMed: 8815919]
9. Börgers C, Kopell N. Synchronization in networks of excitatory and inhibitory neurons with sparse, random connectivity. Neural Comput. 2003; 15:509–538. [PubMed: 12620157]
10. Tiesinga PH, Fellous JM, Salinas E, José JV, Sejnowski TJ. Inhibitory synchrony as a mechanism for attentional gain modulation. J Physiol Paris. 2004; 98:296–314. [PubMed: 16274973]
11. Börgers C, Kopell NJ. Gamma oscillations and stimulus selection. Neural Comput. 2008; 20:383–414. [PubMed: 18047409]
12. Knoblich U, Siegle JH, Pritchett DL, Moore CI. What do we gain from gamma? Local dynamic gain modulation drives enhanced efficacy and efficiency of signal transmission. Front Hum Neurosci. 2010; 4:1–12. [PubMed: 20204154]
13. Shadlen MN, Movshon JA. Synchrony unbound: a critical evaluation of the temporal binding hypothesis. Neuron. 1999; 24:67–77. 111–25. [PubMed: 10677027]
14. Ray S, Maunsell JH. Differences in gamma frequencies across visual cortex restrict their possible use in computation. Neuron. 2010; 67:885–896. [PubMed: 20826318]
15. Penttonen M, Kamondi A, Acsady L, Buzsaki G. Gamma frequency oscillation in the hippocampus of the rat: intracellular analysis in vivo. Eur J Neurosci. 1998; 10:718–728. [PubMed: 9749733]
16. Whittington MA, Traub RD, Kopell N, Ermentrout B, Buhl EH. Inhibition-based rhythms: experimental and mathematical observations on network dynamics. Int J Psychophysiol. 2000; 38:315–336. [PubMed: 11102670]
17. Hasenstaub A, Shu Y, Haider B, Kraushaar U, Duque A, McCormick DA. Inhibitory postsynaptic potentials carry synchronized frequency information in active cortical networks. Neuron. 2005; 47:423–435. [PubMed: 16055065]
18. Börgers C, Epstein S, Kopell NJ. Gamma oscillations mediate stimulus competition and attentional selection in a cortical network model. Proc Natl Acad Sci U S A. 2008; 105:18023–18028. [PubMed: 19004759]

19. Cardin JA, et al. Driving fast-spiking cells induces gamma rhythm and controls sensory responses. Nature. 2009; 459:663–667. [PubMed: 19396156]
20. Sohal VS, Zhang F, Yizhar O, Deisseroth K. Parvalbumin neurons and gamma rhythms enhance cortical circuit performance. Nature. 2009; 459:698–702. [PubMed: 19396159]
21. Buzsáki G, Wang XJ. Mechanisms of gamma oscillations. Annu Rev Neurosci. 2012
22. Moore CI, Carlen M, Knoblich U, Cardin JA. Neocortical interneurons: from diversity, strength. Cell. 2010; 142:189–193. [PubMed: 20655460]
23. Traub RD, Whittington MA, Colling SB, Buzsáki G, Jefferys JG. Analysis of gamma rhythms in the rat hippocampus in vitro and in vivo. J Physiol. 1996; 493(Pt 2):471–484. [PubMed: 8782110]
24. Cardin JA, et al. Targeted optogenetic stimulation and recording of neurons in vivo using cell-type-specific expression of Channelrhodopsin-2. Nat Protoc. 2010; 5:247–254. [PubMed: 20134425]
25. Carlén M, et al. A critical role for NMDA receptors in parvalbumin interneurons for gamma rhythm induction and behavior. Mol Psychiatry. 2011
26. Cohen JD, Castro-Alamancos MA. Detection of low salience whisker stimuli requires synergy of tectal and thalamic sensory relays. J Neurosci. 2010; 30:2245–2256. [PubMed: 20147551]
27. Miyashita T, Feldman DE. Behavioral detection of passive whisker stimuli requires somatosensory cortex. Cereb Cortex. 2013; 23:1655–1662. [PubMed: 22661403]
28. Sachidhanandam S, Sreenivasan V, Kyriakatos A, Kremer Y, Petersen CC. Membrane potential correlates of sensory perception in mouse barrel cortex. Nat Neurosci. 2013; 16:1671–1677. [PubMed: 24097038]
29. Hamada Y, Miyashita E, Tanaka H. Gamma-band oscillations in the “barrel cortex” precede rat's exploratory whisking. Neuroscience. 1999; 88:667–671. [PubMed: 10363807]
30. Sirota A, Montgomery S, Fujisawa S, Isomura Y, Zugaro M, Buzsáki G. Entrainment of neocortical neurons and gamma oscillations by the hippocampal theta rhythm. Neuron. 2008; 60:683–697. [PubMed: 19038224]
31. Jones MS, Barth DS. Sensory-evoked high-frequency (gamma-band) oscillating potentials in somatosensory cortex of the unanesthetized rat. Brain Res. 1997; 768:167–176. [PubMed: 9369313]
32. Shaw FZ, Chew JH. Dynamic changes of gamma activities of somatic cortical evoked potentials during wake-sleep states in rats. Brain Res. 2003; 983:152–161. [PubMed: 12914976]
33. Adesnik H, Scanziani M. Lateral competition for cortical space by layer-specific horizontal circuits. Nature. 2010; 464:1155–1160. [PubMed: 20414303]
34. Shao YR, et al. Plasticity of recurrent l2/3 inhibition and gamma oscillations by whisker experience. Neuron. 2013; 80:210–222. [PubMed: 24094112]
35. Baranauskas G, et al. Origins of 1/f2 scaling in the power spectrum of intracortical local field potential. J Neurophysiol. 2012; 107:984–994. [PubMed: 22090461]
36. Jia X, Tanabe S, Kohn A. Gamma and the coordination of spiking activity in early visual cortex. Neuron. 2013; 77:762–774. [PubMed: 23439127]
37. Börgers C, Epstein S, Kopell NJ. Background gamma rhythmicity and attention in cortical local circuits: a computational study. Proc Natl Acad Sci U S A. 2005; 102:7002–7007. [PubMed: 15870189]
38. Ritt JT, Andermann ML, Moore CI. Embodied information processing: vibrissa mechanics and texture features shape micromotions in actively sensing rats. Neuron. 2008; 57:599–613. [PubMed: 18304488]
39. Wolfe J, Hill DN, Pahlavan S, Drew PJ, Kleinfeld D, Feldman DE. Texture coding in the rat whisker system: slip-stick versus differential resonance. PLoS Biol. 2008; 6:e215. [PubMed: 18752354]
40. Pinto DJ, Brumberg JC, Simons DJ. Circuit dynamics and coding strategies in rodent somatosensory cortex. J Neurophysiol. 2000; 83:1158–1166. [PubMed: 10712446]
41. Gerdjikov TV, Bergner CG, Stüttgen MC, Waiblinger C, Schwarz C. Discrimination of vibrotactile stimuli in the rat whisker system: behavior and neurometrics. Neuron. 2010; 65:530–540. [PubMed: 20188657]

42. Jadhav SP, Wolfe J, Feldman DE. Sparse temporal coding of elementary tactile features during active whisker sensation. Nat Neurosci. 2009
43. Gross J, Schnitzler A, Timmermann L, Ploner M. Gamma oscillations in human primary somatosensory cortex reflect pain perception. PLoS Biol. 2007; 5:e133. [PubMed: 17456008]
44. Fellous M, Rudolph M, Destexhe A, Sejnowski J. Synaptic background noise controls the input/output characteristics of single cells in an in vitro model of in vivo activity. Neuroscience. 2003; 122:811–829. [PubMed: 14622924]
45. Rudolph M, Pospischil M, Timofeev I, Destexhe A. Inhibition determines membrane potential dynamics and controls action potential generation in awake and sleeping cat cortex. J Neurosci. 2007; 27:5280–5290. [PubMed: 17507551]
46. O'Connor DH, et al. Neural coding during active somatosensation revealed using illusory touch. Nat Neurosci. 2013
47. Histed MH, Maunsell JH. Cortical neural populations can guide behavior by integrating inputs linearly, independent of synchrony. Proc Natl Acad Sci U S A. 2014; 111:E178–E187. [PubMed: 24367105]
48. Doron G, von Heimendahl M, Schlattmann P, Houweling A, Brecht M. Spiking Irregularity and Frequency Modulate the Behavioral Report of Single-Neuron Stimulation. Neuron. 2014; 81:653–663. [PubMed: 24507196]
49. Lee SH, et al. Activation of specific interneurons improves V1 feature selectivity and visual perception. Nature. 2012; 488:379–383. [PubMed: 22878719]
50. Engel AK, Singer W. Temporal binding and the neural correlates of sensory awareness. Trends Cogn Sci. 2001; 5:16–25. [PubMed: 11164732]
51. Boyden ES, et al. Millisecond-timescale, genetically targeted optical control of neural activity. Nat Neurosci. 2005; 8:1263–1268. [PubMed: 16116447]
52. Nguyen DP, et al. Micro-drive array for chronic in vivo recording: tetrode assembly. J Vis Exp. 2009
53. Voigts J, Siegle JH, Pritchett DL, Moore CI. The flexDrive: An ultra-light implant for optical control and highly parallel chronic recording of neuronal ensembles in freely moving mice. Front Sys Neurosci. 2013; 7
54. Yizhar O, et al. Neocortical excitation/inhibition balance in information processing and social dysfunction. Nature. 2011; 477:171–178. [PubMed: 21796121]
55. Siegle JH. Combining optical stimulation with extracellular electrophysiology in behaving mice. Neuronal Network Analysis. 2012
56. Carvell GE, Simons DJ. Membrane potential changes in rat SmI cortical neurons evoked by controlled stimulation of mystacial vibrissae. Brain Res. 1988; 448:186–191. [PubMed: 3390715]
57. Armstrong-James M, Fox K, Das-Gupta A. Flow of excitation within rat barrel cortex on striking a single vibrissa. J Neurophysiol. 1992; 68:1345–1358. [PubMed: 1432088]
58. Moore CI, Nelson SB. Spatio-temporal subthreshold receptive fields in the vibrissa representation of rat primary somatosensory cortex. J Neurophysiol. 1998; 80:2882–2892. [PubMed: 9862892]
59. Brecht M, Roth A, Sakmann B. Dynamic receptive fields of reconstructed pyramidal cells in layers 3 and 2 of rat somatosensory barrel cortex. J Physiol. 2003; 553:243–265. [PubMed: 12949232]
60. Tolias AS, Ecker AS, Siapas AG, Hoenselaar A, Keliris GA, Logothetis NK. Recording chronically from the same neurons in awake, behaving primates. J Neurophysiol. 2007; 98:3780–3790. [PubMed: 17942615]
61. Schmitzer-Torbert N, Jackson J, Henze D, Harris K, Redish AD. Quantitative measures of cluster quality for use in extracellular recordings. Neuroscience. 2005; 131:1–11. [PubMed: 15680687]
62. Davidson TJ, Kloosterman F, Wilson MA. Hippocampal replay of extended experience. Neuron. 2009; 63:497–507. [PubMed: 19709631]
63. Goldberg JM, Brown PB. Response of binaural neurons of dog superior olivary complex to dichotic tonal stimuli: some physiological mechanisms of sound localization. J Neurophysiol. 1969; 32:613–636. [PubMed: 5810617]
64. Kumbhani RD, Nolt MJ, Palmer LA. Precision, reliability, and information-theoretic analysis of visual thalamocortical neurons. J Neurophysiol. 2007; 98:2647–2663. [PubMed: 17581854]

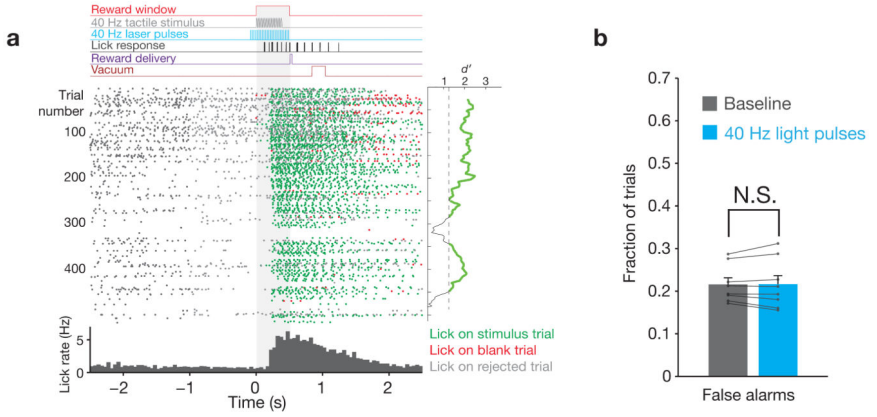

Figure 1. Task structure

a, Top: Structure of an example trial, indicating the timing of the vibrissal stimulus relative to laser pulses, licking behavior, and the reward window. Middle: raster plot of lick times for an example session, aligned to the start of the reward window (gray shading). Each dot indicates a single lick, with color representing the trial type (hit, false alarm, or rejected). The mean d' calculated over 50-trial periods is shown to the right of the raster plot, with the threshold of 1.25 indicated. Bottom: Histogram of lick times for this session. **b**, The falsealarm rate on trials with and without light presentation (N = 8 mice, 141,343 total trials, error bars indicate mean ± s.e.m.) indicate that mice did not respond to optical stimulation. Values for individual mice are superimposed in black.

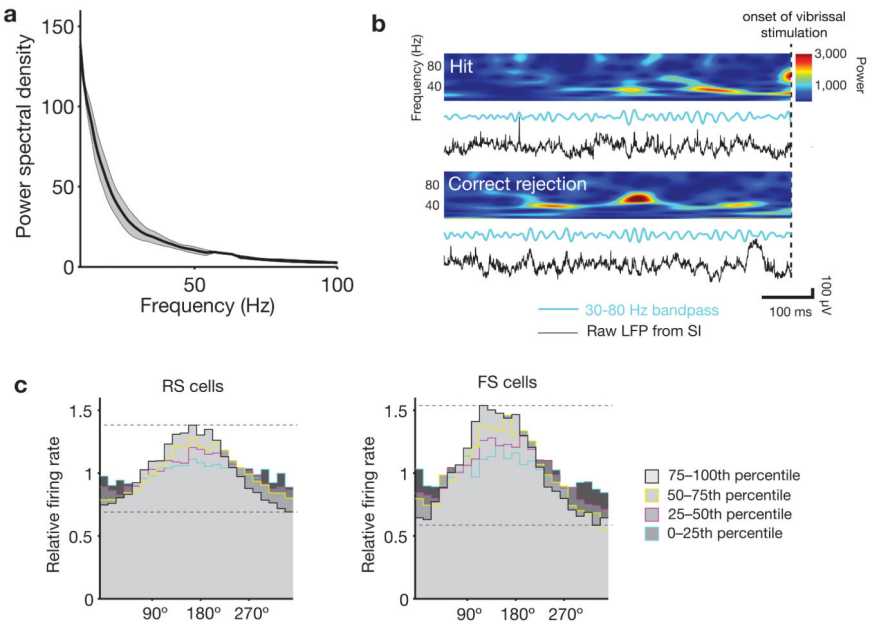

Figure 2. Gamma is expressed in distinct bouts of activity in the local field potential (LFP), associated with enhanced phase locking of spiking activity

a, Average LFP power spectral density for 3 electrodes from 3 mice (multi-taper spectra with time-bandwidth product of 3 and taper count of 5, computed over 2 s pre-stimulus intervals for an entire session, error bars indicate mean ± s.e.m.). A peak in the gamma band is not apparent when averaging over these longer intervals. **b**, In contrast, when more refined temporal analyses are applied (see text), spontaneously arising bouts of ~40 Hz oscillations in the local field potential are common during the pre-stimulus period. Such events are apparent in the time-frequency spectrograms (top), band-passed LFP (blue lines), and raw LFP (black lines), and occurred approximately once per second. See also Supplementary Fig. 1 for examples from all mice. **c**, Single-unit cycle histograms normalized by baseline firing rate and plotted as a function of the endogenous level of 30–80 Hz oscillations in the pre-stimulus period. Each detected interval was sorted into quartiles based on the amplitude of the LFP signal filtered in the gamma band. Periods with the highest gamma power (75^{th}–100^{th} percentile) show the highest modulation of spike activity. Units were classified as regular-spiking (RS) or fast-spiking (RS) according to their peak-to-trough ratio and spread (Supplementary Fig. 4).

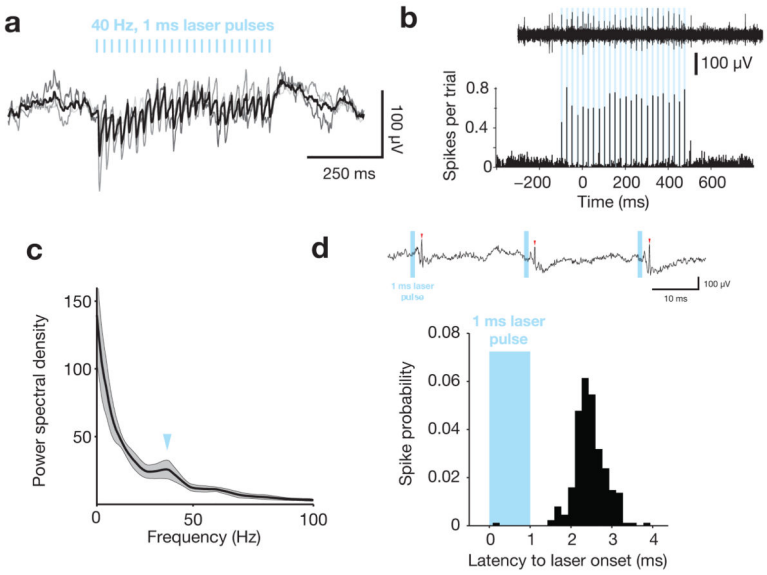

Figure 3. Optogenetic stimulation to emulate FS-gamma

a, The mean (thick line) and individual (thin lines) light-evoked responses in the input-inverted (spikes positive) local field potential to 40-Hz optogenetic drive of FS. Thin black lines represent mean response for each of 3 mice, thick black line represents the average across mice; vertical blue lines indicate timing of 1 ms laser pulses. **b**, An example of light-evoked spikes from a single trial (top) and the average of 96 trials from a single session (bottom). Vertical blue lines indicate timing of 1 ms laser pulses. **c**, Average LFP power spectral density for 3 electrodes from 3 mice, computed using the same parameters as Fig. 2a, except during epochs of 40 Hz laser pulses only. **d**, Example of a well-isolated, light-driven FS cell, showing an unfiltered trace with identified spikes (top) and histogram of spikes relative to laser onset (bottom). The vast majority of spikes occur between 2 and 3 ms after the start of the light pulse, replicating prior findings in anesthetized mice[19].

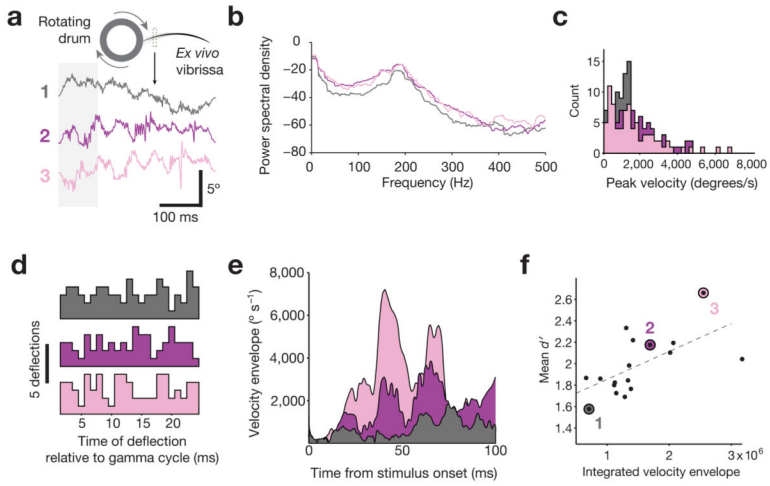

Figure 4. Generation and characterization of naturalistic vibrissal stimuli

a, Movements of an *ex vivo* B2 vibrissa during contact with a sandpaper-covered rotating drum were recorded to obtain naturalistic stimulation patterns (3 examples shown here, see text for details). **b**, Power spectral densities (dB units) computed for the three naturalistic stimuli shown in panel a, revealing a peak at ∼200 Hz. **c**, Histograms of the peak micro-motion velocities for all deflections in the three example waveforms. The range is comparable to velocities measured from the vibrissae of freely behaving rats[38]. **d**, Distribution of deflections within cycles of optogenetically entrained gamma. For each stimulus, deflections with a peak velocity over 100°/s were aligned according to their latency from pulses of 40 Hz light. These high-velocity micro-motion events were evenly distributed throughout the gamma cycle, preventing any preferential phase alignment. **e**, Velocity envelope of the 3 naturalistic stimuli shown in panel a. **f**, Relationship between the integrated velocity envelope for the first 100 ms of each naturalistic stimulus and the mean detectability of that stimulus across $N = 4$ mice (1981 total trials), detection rates for the 3 traces shown in panel a are indicated.

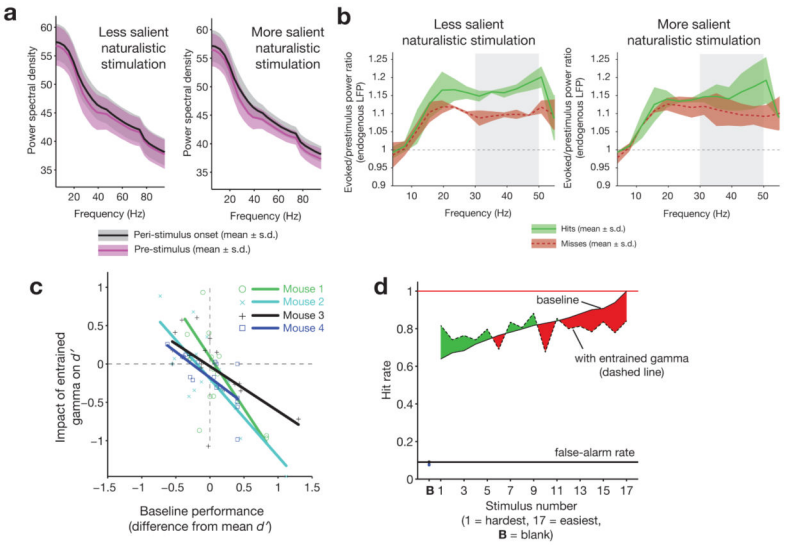

Figure 5. Endogenous and entrained FS-gamma predict enhanced detection of less salient naturalistic stimuli

a, Baseline versus evoked power spectra, for both less salient and more salient naturalistic stimuli. Error bars indicate mean ± s.e.m. **b**, Endogenous peri-stimulus spectral power in the gamma range during detection of less salient (left, mean of naturalistic stimuli across mice with baseline detectability levels below the median) and most salient (right, above the median) naturalistic stimuli, shown for hit (green) and miss (red) trials. Only for less salient stimuli did power in the 30–50 Hz range (gray bar) differ between hits and misses (red and green shaded regions represent mean ± s.e.m). **c**, Relationship between baseline (laser off) performance and the effect of optogenetically entrained FS-gamma on d' (N = 17 stimuli presented to 4 mice). All mice displayed enhanced detection of less salient natural stimuli and a significant correlation between detectability and the entrained impact of FS-gamma (Mouse 1, R^2 = 0.47, P = 0.0024; Mouse 2, R^2 = 0.66, P = 0.001; Mouse 3, R^2 = 0.38, P = 0.008; Mouse 4, R^2 = 0.54, P = 0.0008). **d**, Average impact of entrained gamma on detection of stimuli ordered by detectability. For each mouse, the 17 natural stimuli were sorted as a function of detectability for that animal and then the impact of FS-gamma on these ordinal rankings were summed across animals. The difference between detection performance with and without entrained gamma is indicated in green (enhanced performance) or red (impaired performance).

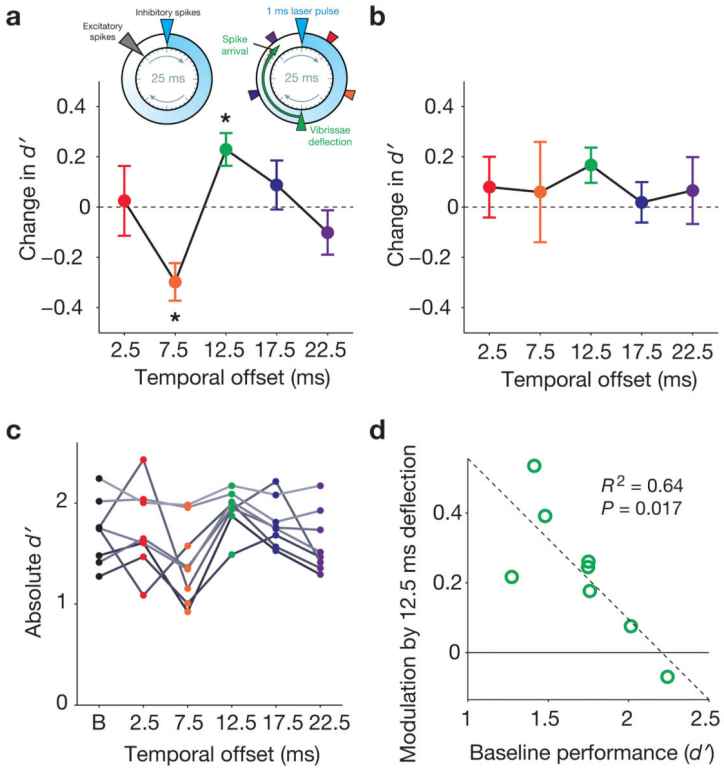

Figure 6. Entrained FS-gamma enhances detection of less salient periodic stimuli at a specific optimal temporal offset between FS synchronization and sensory drive

a, The inset on the upper left summarizes the findings of prior studies[8-12,17,19,22] showing that FS-gamma creates a window of opportunity for optimal excitatory firing immediately prior to a subsequent FS synchronization event. For a 40 Hz gamma rhythm, this cycle repeats every 25 ms. The inset on the upper right illustrates the temporal offsets between optogenetic light pulses and vibrissae deflections used in this study. Vibrissa stimulation 12.5 ms after FS synchronization (green triangle) will cause stimulus-evoked neocortical excitation to occur in this window of opportunity, reinforcing the endogenous pattern of FS-gamma expression. The main plot shows the relationship between temporal offset of vibrissal stimulation and difference in *d′* from baseline for $N = 8$ mice (threshold stimulus intensity trials only, see Figure 1). The temporal offset was a significant modulator of response ($P = 0.0016$, Friedman test), with a significant change relative to the "no laser" condition for 7.5 and 12.5 ms offsets (see text for exact *P*-values). **b**, Same as in b, but for trials on which the maximal, highly salient amplitude stimulus was presented. There was no significant effect of changing the temporal offset for detection of these stimuli ($P = 0.711$, Friedman test). **c**, Absolute *d′* values for individual mice (B = baseline "no laser" condition; different shades of gray are used to distinguish individuals). **d**, Relationship between baseline performance and *d′* modulation by the 12.5 ms temporal offset condition for individual mice. In all plots, error bars indicate mean ± s.e.m.

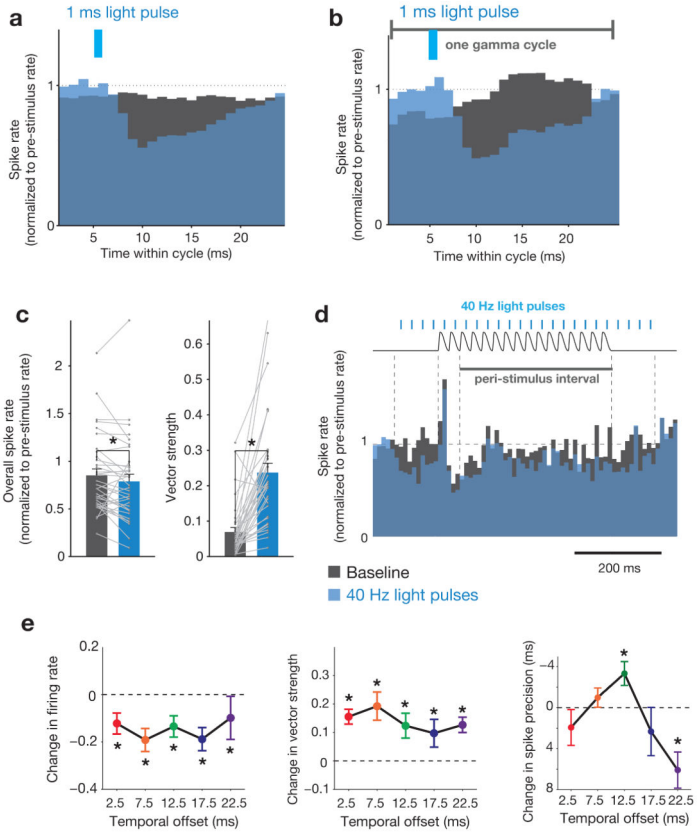

Figure 7. Interaction between optogenetically entrained gamma and the response to vibrissal deflections

a, Mean peri-stimulus (naturalistic stimulation) spike histogram averaged over individual cycles of optogenetically entrained gamma for $N = 35$ regular-spiking single unitsfrom 3 miceunder two conditions: laser off (black bars) and laser on (blue bars). **b**, Mean spike histogram for periodic stimulation, averaged over individual cycles of gamma, time-locked to laser onset (same units as in a). **c**, Mean changes in firing rate and vector strength for the same units as in a. Firing rate is normalized to pre-stimulus rate. Values for individual cells are overlaid in gray. Error bars indicate mean ± s.e.m. (* = $P < 0.05$, Wilcoxon signed-rank test; $P = 0.0420$ for firing rate, $P = 4.06 \times 10^{-6}$ for vector strength). **d**, Mean peri-stimulus spike histogram for the periodic stimulation condition. Time course of the vibrissae stimulus (black trace, top) and laser pulses (blue lines, top) are superimposed. **e**, Left panel: Change in mean magnitude of the peak evoked response relative to the interval 100 ms prior to stimulus onset with laser stimulation, normalized to the no laser condition, for the five temporal offsets diagrammed in Fig. 6a ($N = 35$ single units from 3 mice; P-values are as follows: 2.5 ms offset, $P = 0.0137$; 7.5 ms offset, $P = 0.0012$; 12.5 ms offset, $P = 0.0059$; 17.5 ms offset, $P = 0.0003$; 22.5 ms offset, $P = 0.0007$). Center panel: Change in vector strength for the same interval ($N = 35$ single units from 3 mice; P-values are as follows: 2.5 ms offset, $P = 7.6 \times 10^{-6}$; 7.5 ms offset, $P = 4.6 \times 10^{-5}$; 12.5 ms offset, $P = 0.00019$; 17.5 ms offset, $P = 0.027$; 22.5 ms offset, $P = 0.00021$). Right panel: Mean spike precision within the first 25 ms of stimulus onset relative to the no laser condition (multi-unit activity for $N =$ 15 electrodes from 3 mice; P-values are as follows: 2.5 ms offset, $P = 0.68$; 7.5 ms offset, P

= 2.27; 12.5 ms offset, P = 0.014; 17.5 ms offset, P = 1.26; 22.5 ms offset, P = 0.0003).* = P< 0.05, Wilcoxon signed-rank test with Bonferroni correction; error bars indicate mean ± s.e.m.